Deliverable Report

Deliverable No: 1.1

Deliverable Title: Report on engineered quantum light sources

Grant Agreement number: 101135288

Project acronym: EPIQUE

Project title: European Photonic Quantum Computer

Project website address: www.quantumepique.eu

Deliverable table

Deliverable no.	1.1
Deliverable name	Report on engineered quantum light sources
WP no.	1
Type	R
Dissemination level	PU
Delivery date from Annex I	Month 12
Actual delivery date	Month 12
Lead beneficiary	UPB
Name and surname of the scientific representative	Prof. Dr. Christine Silberhorn
Email address of the scientific representative	christine.silberhorn@upb.de

D1.1: Report on engineered quantum light sources [M18]
We will develop engineered highbrightness sources of pulsed single-mode (effective mode number $K < 1.05$) and two-mode squeezing in the telecom C band (1535 – 1565nm). We will investigate both KTP and TF LNOI to generate pulsed squeezing of more than 10dB in single pass with pulse durations in the picosecond regime, ideal for fibre integration. Operating the sources at low squeezing levels will facilitate the generation of high-quality heralded single photons.

Description of work carried out for D1.1

Executive summary

During the first year of the project, we have investigated pulsed sources of squeezed light with picosecond pulse duration for use in photonic quantum computing. We considered two material platforms: postassium titanyl phosphate (KTP) and thin-film lithium niobate (TFLN). While KTP is an established material for the generation of high-quality squeezed states at telecommunications wavelengths, TFLN holds the promise of improved device integration and, potentially, higher source efficiency. We found, however, that TFLN devices suffer from insufficient interfacing efficiency due to their small mode size originating from the strong confinement and sub-micron feature sizes. Although being a promising candidate for future sources, we decided to focus on integrated KTP sources for this project due to their, as of now, superior overall performance.

We have realized an optimized squeezing source based on type-II parametric down-conversion (PDC) in periodically poled KTP waveguide. The source operates in a close-to-single-spectral-mode regime, which is verified with an effective mode number of $K \approx 1.1$. It generates pulsed single-mode or two-mode squeezing, set by the user, at a central wavelength around 1550 nm and a pulse duration of around 4 ps. Finally, our source features an extreme brightness of more than 40,000 generated photon pairs per pump pulse, which translates to significantly more than 10 dB generated squeezing.

Our source fulfills the demanding requirements of the project and will be utilized for upcoming demonstrations of photonic quantum computing in UPB's time-multiplexed platform.

The photonic platform is in general capable of implementing universal quantum computation. First real world applications and demonstrations of this platform focus on the so called noisy-intermediate-scale quantum (NISQ) regime. Gaussian boson sampling (GBS) [1] is a promising NISQ platform and has a variety of relevant applications from demonstrating quantum advantage [2, 3] to simulating quantum chemistry [4]. A typical GBS setup consists of three sections: the quantum light source, a programmable linear optical network implementing an arbitrary unitary and a photon number resolving detector.

I. QUANTUM LIGHT SOURCES FOR GAUSSIAN BOSON SAMPLING

Fundamentally GBS requires squeezed light as a quantum resource. A single-mode squeezed light field is generally described using the unitary squeezing operator

$$\hat{S}(\xi) = e^{\left(\frac{\xi}{2}\hat{a}^\dagger\hat{a}^\dagger - \frac{\xi^*}{2}\hat{a}\hat{a}\right)} \tag{1}$$

where $\xi = re^{i\varphi}$ is the squeezing parameter, $r \in \mathbb{R}_+$ the squeezing strength and $\varphi \in [0, 2\pi]$ the squeezing angle. If this operator acts on the vacuum field, the resulting optical field is called single-mode squeezed vacuum light which can be displaced using coherent laser light.

An important property of these fields is that two single-mode squeezed states become photon number entangled if they are combined on a $50:50$ beamsplitter (BS). This results in the creation of a two-mode squeezed state, if the phases of the two single-mode squeezed states are set appropriately. Now we can describe one of the beamsplitter ports as mode A and the other as mode B with their respective creation operators $\hat{a}^\dagger$ and $\hat{b}^\dagger$. The resulting squeezing operator describing a two-mode squeezed

$$\hat{S}^{(2)}_{A,B}(\xi) = e^{\left(\frac{\xi}{2}\hat{a}^\dagger\hat{b}^\dagger - \frac{\xi^*}{2}\hat{a}\hat{b}\right)} \tag{2}$$

can similarly be transformed via the same balanced BS into two independent single-mode squeezed states. On the other hand, such a two-mode squeezed states has the interesting property of perfect photon number correlations between both fields, typically called signal and idler. This can be used to generate heralded Fock states, where a photon number resolving measurement on one fields determines the number of photons in the other. In the low gain regime this allows for the creation of heralded single-photons with high purity.

Both single- and two-mode squeezed fields can be created using the non-linear optical process parametric down conversion (PDC). Here we consider so-called type

II PDC based sources for two-mode squeezed light in the telecommunications C band (1535 nm - 1565 nm) as this allows compatibility with fibre based architecture, low losses and the utilisation of existing telecommmunications technology.

A. Parametric Down Conversion

The squeezing operator can be realized via parametric down-conversion (PDC). PDC is a three wave mixing process in a $\chi^{(2)}$ non-linear optical medium where a photon with high energy E_p decays into two lower energetic photons called signal and idler. Here we employ a type-II PDC process which means that the idler and signal photon are produced in orthogonal modes. We consider the idler photon to be generated in the horizontal (H) polarization and the signal photon in vertical (V) polarization. The underlying interaction Hamiltonian is

$$\hat{H} = \Gamma \hat{a}_p \hat{a}_s^\dagger \hat{a}_i^\dagger + \text{h.c.} \tag{3}$$

where $\hat{a}_p$, $\hat{a}_s^\dagger$, and $\hat{a}_i^\dagger$ are the creation and annihilation operators acting on the pump (p), signal (s) and idler (i) field respectively. The parameter Γ describes the interaction strength between all three fields and depends strongly on the underlying $\chi^{(2)}$ non-linearity and the field overlaps. Under the assumption of a strong coherent laser as the pump field, $\hat{a}_p$ can be approximated as the field amplitude $\alpha_p \in \mathbb{C}$.

For this process to occur the following two conditions have to be met: the process must obey the conservation of energy, meaning that the converted pump photons energy E_p must be equal to the sum of the created idler and signal photons energies E_i and E_s. This is given by

$$E_p = E_s + E_i = \hbar\omega_s + \hbar\omega_i = \hbar\omega_p \tag{4}$$

where ω_p is the angular frequency of the pump field and ω_s and ω_i are the angular frequencies of the signal and idler field, respectively. Here we consider a pulsed laser as the pump field with the average field strength of $|\alpha|^2$ per pulse. Using a pulsed laser allows to perform time-multiplexed operations and increases the field strength with decreasing pulse duration. This is advantageous as the combined interaction strength $\zeta = \Gamma\alpha_p$ scales with the amplitude of the pump field present. As a side note, a pulsed pump is also crucial to achieve single-spectral-mode operation, as will be detailed below. Following from the energy conservation condition, we can calculate all possible combinations of idler and signal field angular frequency for all angular frequencies present in the pump field individually. From there we can calculate the pump distribution as:

$$\alpha(\omega_s, \omega_i) = \int A(\omega_p)\delta(\omega_p, \omega_s + \omega_i)d\omega_p \tag{5}$$

where A is the spectral distribution of the pump field. A visualization of the pump distribution is shown in Fig. 1a where it is calculated for a Gaussian distribution centered around 775nm and is displayed in a λ_i-λ_s plot resulting in a $-45°$ line. Secondly, the PDC process must obey momentum conservation, which is given by

$$\hbar\vec{k}_p = \hbar\vec{k}_s + \hbar\vec{k}_i \tag{6}$$

where $\vec{k}_p$, $\vec{k}_s$ and $\vec{k}_i$ are the wave vectors of the pump, signal and idler field respectively. Here we implement the PDC process in a waveguide, restricting the wave vector as well as the intensity profile of the pump, signal and idler fields. The employed single-mode waveguide allows only for one combination of wave vectors to be guided in the material. This increases the field overlap and therefore increases the interaction strength Γ. It furthermore increases the indistinguishably between generated photon pairs as it negates the possibility of spacial multimodenes.

On the other hand, the resulting spatial mode restriction makes it impossible to fulfill the momentum conservation in most materials exhibiting $\chi^{(2)}$ non-linearity. This problem is typically solved by the introducing a third term $\Delta\vec{k}$ into the condition. The resulting momentum conservation, which is commonly called the quasi phase matching condition, can be implemented by engineering the non-linear material. This modification of the condition is achieved using periodic polling where the non-linearity domain of the crystal is periodically inverted. The resulting quasi phase matching condition can be described by

$$k_p = k_s + k_i + \frac{2\pi}{\Lambda} \tag{7}$$

where Λ is the length of the periodically repeated inversions of the non-linearity domain. The resulting phasematching function $\phi(\omega_s, \omega_i)$ has a sinc-shape resulting from the Fourier transformation of the spatially confined interaction length. A visualization of an exemplary quasi phasi matching function is shown in figure 1b where its calculated for a λ_i-λ_s plot resulting in $45°$ line with sinc-distributed side bands.

The combination of the energy conservation and phase matching condition results in the transfer function of the process, known as the Joint Spectral Amplitude (JSA) $f(\omega_s, \omega_i)$:

$$f(\omega_s, \omega_i) = \alpha(\omega_s, \omega_i)\phi(\omega_s, \omega_i) \tag{8}$$

Using the Schmidt decomposition the JSA can be decomposed into a series of orthogonal modes $f_s^{(k)}(\omega_s)$ and $f_i^{(k)}(\omega_i)$ describing the individual spectrum of the signal and idler respectively. In a good approximation, the resulting Hamiltonian can be written as

$$f(\omega_s, \omega_i) = \lambda_k \sum_k f_s^{(k)}(\omega_s) f_i^{(k)}(\omega_i) \tag{9}$$

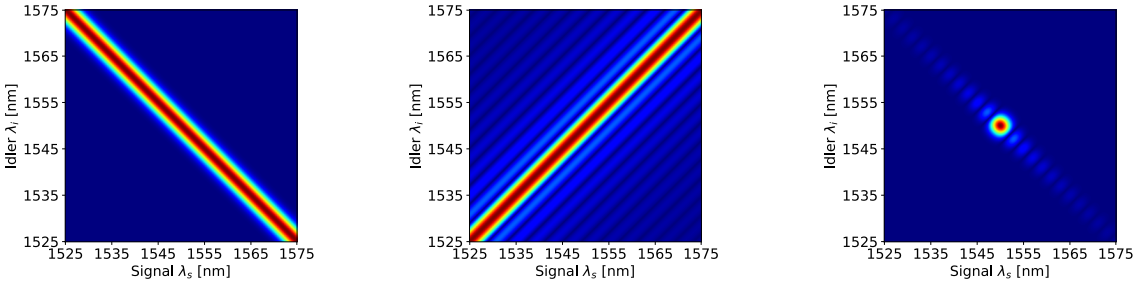

(a) Energy conservation condition under the constraints of a Gaussian spectral distribution for the pump field with a central wavelength of 775nm and standard deviation of 2nm.

(b) Ideal quasi phase matching condition for a periodically poled waveguide. Shows side bands from the underlying sinc-shape with the central band width shaped for maximal degeneracy between idler and signal spectral jsa.

(c) The resulting joint spectral amplitude from the energy conservation and quasi phase matching condition. The central spot exhibits degeneracy for both idler and signal photon at a wavelength of 1550nm.

FIG. 1: Ideal distributions for the energy conservation, quasi phase matching condition and resulting JSA for maximally indistinguishable photons pair generation.

$$\begin{aligned}\Rightarrow \hat{H} &= \tau \sum_k \lambda_k \int d\omega_s f_s^{(k)}(\omega_s)\hat{a}_s^\dagger(\omega_s) \int d\omega_i f_i^{(k)}(\omega_i)\hat{a}_i^\dagger(\omega_i) + \text{h.c.} \\ &= \tau \sum_k \lambda_k \hat{A}_i^\dagger(k)\hat{A}_s^\dagger(k) + \text{h.c.}\end{aligned} \tag{10}$$

where the constant τ is the conglomerate of the different influences on the interaction strength between all three involved fields and λ_k is the amplitude of the individual frequency modes resulting from the Schmidt decomposition. The resulting unitary operator evolving the system according to the Hamiltonian is the evolution operator $\hat{U}$. Under the assumption that the Hamiltonian is approximately constant over the entire non-linear region, the evolution operator $\hat{U}$ takes the following form:

$$\begin{aligned}\hat{U} &= e^{\left(-\frac{i}{\hbar}\int \hat{H}dt\right)} = e^{-\frac{i\tau}{\hbar}\left(\sum_k \lambda_k \hat{A}_i^\dagger(k)\hat{A}_s^\dagger(k) + \text{h.c.}\right)} \\ &= \bigotimes_k e^{\left(\gamma_k \hat{A}_i^\dagger(k)\hat{A}_s^\dagger(k) + \text{h.c.}\right)} \\ &= \bigotimes_k \hat{S}^{(2)}_{A_i(k),A_s(k)}(\gamma_k)\end{aligned} \tag{11}$$

We interpret this such that a general type-II PDC generates many two-mode squeezed states in orthogonal broadband spectral modes, the so-called temporal modes. Optimizing this structure will be the topic of the next section.

B. Requirements for GBS

Not every squeezed state generated via PDC is suitable for implementation in GBS systems. These applications require the utilization of single-mode squeezers that operate in single-spectral mode. These must meet two crucial criteria simultaneously: decorrelation and indistinguishability.

1. *Decorrelation*

Decorrelation means that there are no leftover correlations between the signal and idler fields in any other degree of freedom then the one defining the individual fields. For the discussed PDC type-II process, where signal and idler fields are distinguishable in their polarization, this means that there are no correlations between their respective frequency distributions. This decorrelation can be quantified following the Schmidt decomposition which decomposes the JSA into a correlated set of orthogonal modes $f_s^{(k)}(\omega_s)$ and $f_i^{(k)}(\omega_i)$ for signal and idler respectively. The resulting set of corresponding amplitudes λ_k can then be used to quantify decorrelation. Specifically, if the Schmidt rank which is defined as the amount of nonzero amplitudes $|\{\lambda_k : \lambda_k \neq 0\}|$ is one, then there are no correlations in the frequency degree of freedom between the signal and idler field. The resulting field is then called decorrelated and the corresponding PDC type-II evolution operator takes the form

$$\hat{U} = e^{\gamma \hat{A}_i^\dagger \hat{A}_s^\dagger + \text{h.c.}} = \hat{S}^{(2)}_{A_i,A_s}(\gamma) \tag{12}$$

similar to a textbook example of a two-mode squeezed vacuum state. Decorrelation is an important property for GBS as any remaining correlations reduce the interference between multiple independent two- or single-mode squeezed fields. In order to quantify how close any given state is to optimal decorrelation, we can utilize the Schmidt number K which quantifies the effective mode number and is defined as:

$$K = \frac{1}{\sum_k |\lambda_k|^4} \in [1, \infty[. \tag{13}$$

Note that, a Schmidt number of one requires a Schmidt rank of one and therefore indicates the presence of a perfectly decorrelated field. In general the Schmidt number

quantifies the number of modes with equal amplitudes required to describe the underlying field. To determine the effective number of modes contained within the generated JSA, the standard method is to do second-order auto-correlation measurement $g^{(2)}$ for either the signal or idler beam [5]. The relationship between $g^{(2)}$ and the effective mode number (K) within the generated JSA is then described mathematically by the broadband correlation function $g^{(2)}$ as:

$$g^{(2)} = 1 + \frac{1}{K}. \tag{14}$$

It is worthwhile to note that this can be measured in a loss-insensitive Hanbury-Brown Twiss experiment.

2. Indistinguishability

Indistinguishability is the second important property for a two-mode squeezed state. Under the assumption of decorrelation, the operators acting on the signal $\hat{A}_s^\dagger = \int d\omega_s f_s(\omega_s)\hat{a}^\dagger(\omega_s)$ and idler $\hat{A}_i^\dagger = \int d\omega_i f_i(\omega_i)\hat{a}^\dagger(\omega_i)$ field can still be distinguishable in their respective spectrum $f(\omega)$. This distinguishability limits the interference between signal and idler required in order to transform the two-mode squeezed state produced via the PDC type-II process. Indistinguishability V can be quantified via the overlap of both frequency modes

$$V = \int d\omega f_i(\omega) f_s^*(\omega) \in [0, 1] \tag{15}$$

where $V = 1$ indicates perfect indistinguishablility and $V = 0$ means complete distinguishablility between the signal and idler fields' spectral modes. This visibility is experimentally accessible via the Hong-Ou-Mandel (HOM) interference. The HOM effect is observed when two photons arrive simultaneously at a balanced beam splitter (BS). When the photons are indistinguishable in all their properties except for the input port of the BS, they will bunch together and exit the BS through the same port. Therefore, it leads to a dip in the coincidence detection rate from the two outputs of BS when both photons are indistinguishable. The coincidence probability as a function of a distinguishable parameter, such as time delay τ is given by:

$$p_{\text{coin}}(\tau) = \frac{1}{2} - \frac{1}{2}\iint d\omega_s d\omega_i \, f^*(\omega_i, \omega_s) f(\omega_s, \omega_i) e^{i(\omega_s - \omega_i)\tau} \tag{16}$$

By comparing the coincidence probability where both fields are distinguishable due to for example a time delay time delay $p_{\text{coin}}(\infty)$ and where they are indistinguishable $p_{\text{coin}}(0)$, we can measure the visibility $V = \frac{p_{\text{coin}}(\infty)}{p_{\text{coin}}(\infty) - p_{\text{coin}}(0)}$ directly.

3. Source Efficiency

A third important property for any quantum light source is the source efficiency η. In quantum mechanics, loss can be modelled via a beamsplitter operation with the reflectivity $r = \sqrt{1-\eta}$ interfering the optical field with the vacuum. For squeezed light this results in the effective reduction of the squeezing strength r proportional to the loss $1 - \eta$. Here it is important to note, that in general losses cannot be compensated for by increasing the squeezing strength r. Furthermore amplification is not possible due to the non-cloning theorem, hence why it is crucial to optimize the source efficiency through careful setup design and mode matching.

4. Brightness

Finally it is important to consider the brightness of the PDC process. It is defined as the ratio between the rate of successfully generated down converted photon pairs R_{PP} and the pump power P_{pump} as well as the spectral bandwidth ($\Delta\lambda$) of the generated fields. The normalized brightness

$$B = \frac{R_{PP}}{\Delta\lambda P_{\text{pump}}^2} \tag{17}$$

is typically given with the unit Hz nm^{-1} mW^{-2}. A higher brightness is always preferable, both from an efficiency point of view by generating the highest amount of squeezing with the least amount of pump power and for achieving the highest squeezing strength possible with the available pump laser.

II. PLATFORMS

We proceed with a discussion of the material platform which can be used to implement squeezing sources for GBS. Here we will consider potassium titanyl phosphate (KTP) as the current state of the art and thin-film lithium niobate (TFLN) as the up and coming material platform for integrated quantum optics and compare them in terms of their phase matching, brightness and losses. KTP has been used to demonstrate quantum advantage within a GBS platform both as a bulk crystal source [2] in a spatial context and as a wave guide written source in a time-multiplexed context [4]. TFLN sources are currently under development and have been shown to offer exciting properties [6].

The first thing to note is that as PDC is a second order non-linear process the corresponding conversion efficiency scales with the material's $\chi^{(2)}$ parameter. Both lithium niobate (LN) and KTP have a strong non-linear coefficient $\chi^{(2)}$ reaching 3.4pm/V for periodically poled KTP and over 15pm/V for periodically poled LN. Using x-cut LN, Shi et al. demonstrated that they could achieve

a normalized SHG efficiency of $(4615 \pm 82)\%$ W^{-1} cm^{-2} and broadband normalized brightness for PDC photon pair generation of around 3.1×10^6 Hz nm^{-1} mW^{-2}. This high brightness is aided by the strong mode confinement in TFLN. On the other hand, this strong mode confinement then requires significant effort for end facet coupling as traditional coupling using free space lenses yield only around 10% collection efficiency. Here grating couplers promise around 45% efficiency and inverse waveguide tapers up to 70% for one wavelength [7–9].

To date, no solution for efficient coupling of more than one wavelength (e.g., the pump and the photon wavelengths) has been realized in TFLN. Because of the aforementioned critical impact of source efficiency on the achievable performance key identifiers, we have decided to realize a squeezing source based on KTP waveguide within EPIQUE.

Secondly, using dispersion engineering, the angle of the phase matching function Θ can be tuned within the constraints of the respective material platform. It can approximately be described by the function

$$\Theta = -\mathrm{actan}\left(\frac{v_{g,i}^{-1} - v_{g,p}^{-1}}{v_{g,s}^{-1} - v_{g,p}^{-1}}\right) \tag{18}$$

with $v_{g,i}$, $v_{g,s}$, $v_{g,p}$ as the group velocity of the idler, signal, and pump field. It has been shown, that a positive phase matching angle is key to single-spectral mode operation and thus decorrelation of a PDC state [10]. This requires an ordering of group velocities according to $v_{g,i} < v_{g,p} < v_{g,s}$, where we note that the labeling of signal and idler is arbitrary.

Thanks to its unique dispersion properties, KTP offers a positive phase matching angle of close to 45° for photons at telecommunications wavelengths. LN, on the other hand, is limited to negative phase matching angles and dispersion engineering based on tailoring the dimensions of TFLN waveguides must be employed. Since the dispersion is sensitive to small fabrication intolerances, reliable TFLN sources are out of reach at the moment. This is another driver for the decision to realize the EPIQUE squeezing source in KTP.

III. FIRST GENERATION SOURCE

The squeezing source currently incorporated in UPB's time-multiplexing platform is based on dispersion-engineered type-II PDC in a periodically poled KTP (ppKTP) waveguide, purchased from AdvR. The sample has a total length of 25mm and an effectively poled length specified by the vendor to be around 22 mm. It has been purchased without any anti-reflection coatings resulting in a $7 - 8\%$ end facet reflectivity. Using the so-called Fabry-Perot method, which is a tool for measuring waveguide propagation losses [11], we measured propagation losses of around $1 - 1.2$ dB/cm. After applying antireflective end-facet coatings in house, we estimate the complete efficiency of the source to be around 70%. This value is extracted from a measurement of the so-called Klyshko efficiency, which is a measure of the efficiency from the source to the detection. Backing out detection efficiency and fiber coupling losses yield the aforementioned 70%. This matches with the predicted propagation losses when assuming that, on average, down-converted photons are produced in the middle of the sample ($-1.2\,\mathrm{dB/cm} \cdot 1\,\mathrm{cm} \approx 75.9\%$). The type-II PDC process in the ppKTP waveguide has been engineered such that the signal and idler fields are produced with orthogonal polarization at around 1540nm allowing for the creation of decorrelated and indistinguishable squeezed light fields. The resulting simulated JSA is displayed In Fig. 2a.

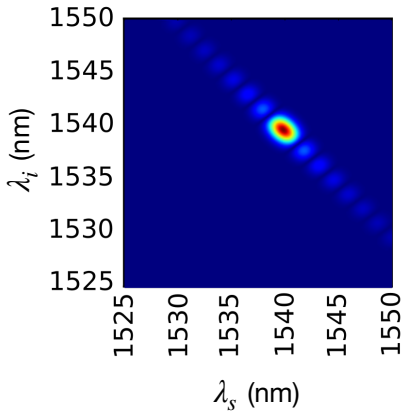

(a) Simulated JSA for the engineered ppKTP waveguide

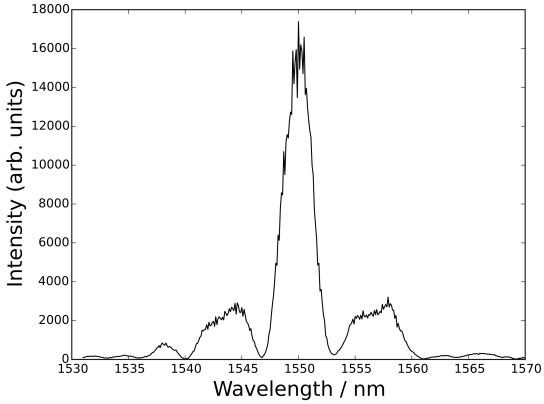

(b) Measured SHG spectrum for WG 1.1

FIG. 2: Inferred spectral properties of the generated field using material simulations for the JSA and second harmonic measurements.

Here a structure oriented at $-45°$ in the (λ_i, λ_s)-plot with a roughly circular region of high intensity is visible. While the angled structure is a characteristic deriving from the energy conservation condition, the high intensity region centered around the degeneracy point where $\lambda_s = \lambda_i$ depends on the relative width of the pump spectrum and phase matching function. We note that the

oscillations are caused by the sinc-shape of the phase matching function, which can be reduced by apodization [12, 13]. As we seek to generate spectrally decorrelated signal-idler pairs, we are only interested in the central high intensity part of the JSA. Experimentally we utilize a pump laser producing pulses with duration of around 3 ps at a wavelength of 772.5 nm and a bandwidth of approximately 0.3 nm.

In order to evaluate the suitability of the spectral properties for our purposes, we conduct second harmonic generation (SHG) measurements to probe the phase matching of the waveguides. Only about one third of the waveguides exhibits a measurable SHG signal in the range from 1530 to 1570 nm. Out of these waveguides only one (WG 1.1) exhibits a spectrum that resembles the expected sinc^2-shape. The recorded spectrum is shown in Fig. 2b, showing a central (degeneracy) wavelength of 1550.12 nm and a bandwidth $\Delta\lambda_{f/2} = 0.9$ nm.

We probe the spectrum of the actually generated PDC photons using a time-of-flight (ToF) spectrometer [14]. To do so, we couple the signal field to dispersive fibers and then utilize superconducting single photons detectors (SNSPDs) to record a histogram of arrival times. The setup is built in such a way that time differences of 1 ns correspond to a wavelength difference of 0.862 nm. The recorded ToF PDC spectra without filtering and with a narrowband bandpassfilter, which transmits only the central peak of the JSA, are shown in Fig. 3a and 3b, respectively.

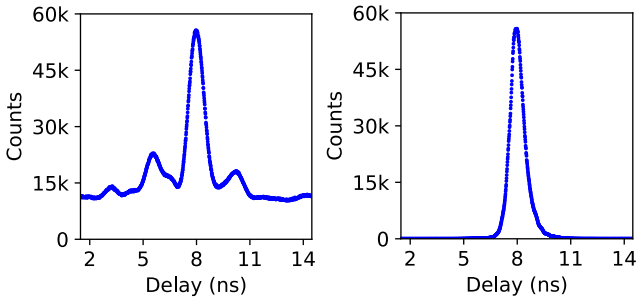

(a) Unfiltered ToF PDC spectrum

(b) Filtered ToF PDC spectrum

FIG. 3: Spectral properties of the produced photons directly measured using a time of flight (ToF) approach.

The unfiltered spectrum at the degeneracy point shows the central peak expected from the simulated JSA as well as the expected side lobes form the sinc-shape of the phase-matching function. We estimate the FWHM for the central peak to be around 1.1nm, hence we insert a 1.8nm bandpass filter to suppress the side lobes. The resulting filtered spectrum has no visible remains of these side-peaks approximating a decorrelated PDC process. Following unheralded $g^{(2)}$ measurements yielded $g^{(2)} \approx 1.7$, which confirms good decorrelation.

Finally, we verify the indistinguishability of the signal and idler fields. For this purpose, we perform HOM-Interference in the low gain regime resulting in a mean photon number per pulse of $\langle n \rangle \approx 0.01$. This ensures that on average there are no more than two photons present, with one in the signal and one in the idler arm. Using a motorized delay stage as well as a balanced beam splitter, we perform a temporal scan of the HOM dip as displayed in Fig. 4. We observe the characteristic dip expected from HOM interference with a visibility of $V \approx 98\%$, from which we conclude an excellent degree of spectral indistinguishability for the generated signal and idler field.

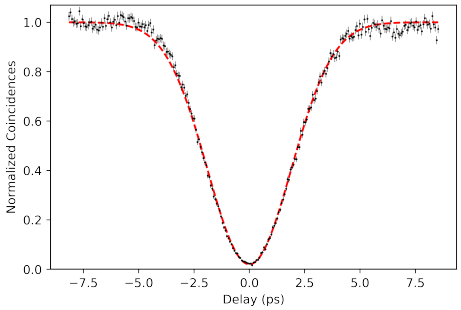

FIG. 4: HOM interference scan.

IV. SECOND GENERATION SOURCE

The next step of the project is to upgrade the source. Here, we will utilize a source similar to the squeezing source built for the Paderborn Quantum Sampler (PaQS), a Gaussian boson sampler based on a spatial network. The source is also based on a ppKTP waveguide with a length of 20mm, purchased from AdvR. The measured waveguide propagation losses are around 0.2db/cm resulting in an expected source efficiency of around 87%, including the reflectivities of the uncoated end facets ($-0.2\,\mathrm{dB} \cdot 92\% \approx 87\%$). Using an SFG process, we measured the phase matching function directly as displayed in Fig. 5a.

The measured phase matching function with an angle of approximately 58° allows for the creation of close-to decorrelated signal and idler fields with an excellent Schmidt number of around $K_{\mathrm{Theory}} \approx 1.1$. We further select a narrowband bandpass filter of around 2 nm to suppress side band generation and background photons.

Continuing with the type-II PDC process, we utilize a pulsed frequency comb laser (Menlo Systems) operating at a centre wavelength of 772.5 nm with a pulse duration of 3 ps, a repetition rate of 80 MHz and a power density of 1.2 W/nm as our pump. With the high brightness of our source, this strong pump laser matched to our source allows us to generate extremely strong squeezing with mean photon numbers in the tens of thousands per pulse. Figure 6 shows that with this source we can push into the non-linear regime of the PDC process, which

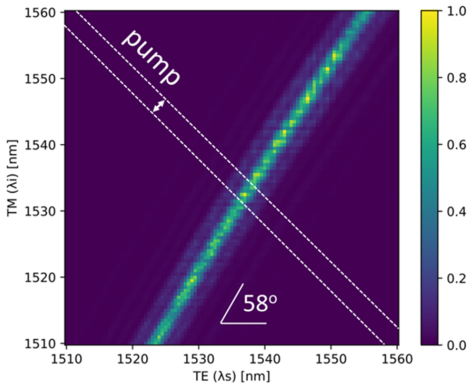

(a) SFG generation when the two input lasers are scanned. The phase-matching angle for 1550 nm is approximately 58 degrees.

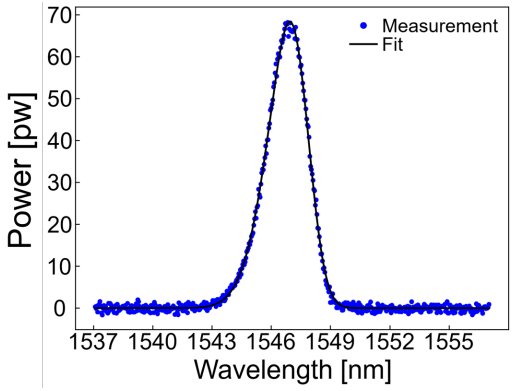

(b) Direct optical spectrum measured by a standard photodiode inside the optical spectrum analyzer (OSA).

FIG. 5: Spectral investigation of the generated PDC light.

features extreme mean photon numbers.

At low pump powers we observe a photon pair generation rate of about 20 pairs/nJ. Pushing past 100 pJ pump pulse energy the non-linear behaviour is clearly visible with the generation of above 40,000 photons at 500 pJ pump pulse energy. This translates to a squeezing strength of $r \approx 6$ and a generated quadrature squeezing of more than 20 db. Note however, that we cannot measure this squeezing directly and the given value is retrieved from the detected photon number. At a repetition rate of 1 MHz generating PDC states with a mean photon number in the tens of thousands results in an average power in the regime of a few Nanowatts. This allows for the direct characterization of the down converted field spectrum using an optical spectrum analyser (OSA). The measured spectrum is displayed in Fig 5b.

Characterisations of the decorrelation between signal and idler field using unheralded $g^{(2)}$ measurements over varying pump band width show values of $g^{(2)} \geq 1.9$ as displayed in Fig 7. The resulting Schmidt numbers of $K < 1.1$ are in excellent agreement with the expectations form the measured phase matching function. This nearly

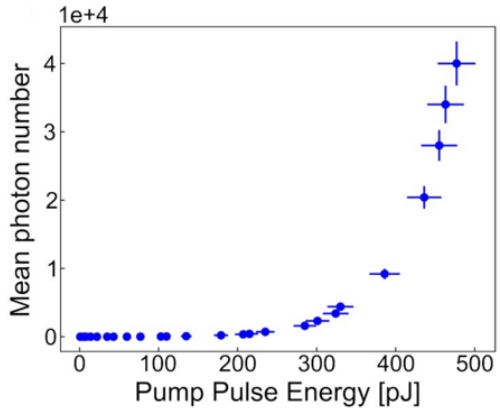

FIG. 6: Nonlinear growth of the mean photon number generated inside the waveguide as the pump pulse energy increases.

completely decorrelated source has also been tested using a heralded HOM-dip between two independent PDC processes from the same source resulting in visibilities of $V \geq 60\%$. Note that this number is limited by the mean photon number used during the measurement and that the $g^{(2)}$ is expected to provide a better estimate of decorrelation for this source.

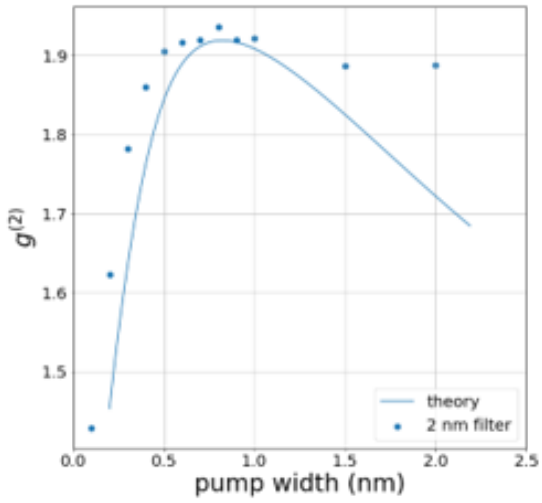

FIG. 7: Dependence between $g^{(2)}$ and the pump width. The second-order auto-correlation function $g^{(2)}$ of the signal mode depends on the pump pulse width, which is precisely adjusted using a spatial light modulator (SLM).

Finally, we verified the indistinguishability of the signal and idler field using HOM-interference in the low gain regime. To this end, we realize so-called polarization HOM-interference. A concatenation of a half-wave plate and polarizing beam splitter in the join arm of signal and idler facilitates the realization of arbitrary beam splitter reflectivities. The resulting coincidence probabil-

	First generation source	Second generation source
Decorrelation		
Broadband correlation function $g^{(2)}$	1.7	> 1.9
Effective modenumber K	1.4	< 1.1
Heralded HOM visibility	80%	$> 60\%$
Photon indistinguishability		
Signal-Idler-HOM visibility	98%	97%
Source efficiency		
Propagation losses	$1 - 1.2$db/cm	0.2db/cm
Source efficiency	70%	87% (w/ end facet coating 95%)
Source brightness		
Photon pairs/pump pulse	≈ 1	> 40000
Generated squeezing	≈ 7.5 dB	> 20dB

TABLE I: Overview table comparing the important source characteristics for our first and second order generation source implemented in a ppKTP waveguide.

ity is plotted in Fig 8. Here we see a visibility exceeding 96% demonstrating the high indistinguishability between signal and idler.

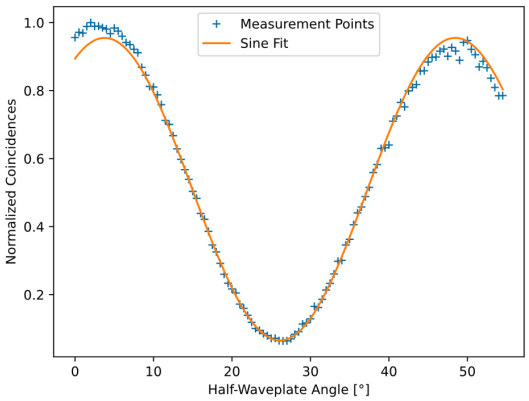

FIG. 8: HOM effect when the input polarization is varied. The coincidence count rate between the two PBS outputs changes with the HWP angle setting.

V. SUMMARY AND JUSTIFICATION FOR DELIVERING D1.1

We have realized a first generation source that is capable of generating highly indistinguishable two-mode squeezed states. These can be used as a source for heralded single photon states, post selected two-photon states, or single-mode squeezed states with moderate squeezing. This source therefore allows for the implementation of linear optical networks with few input photons and has been used to demonstrate a post selected two-photon time-multiplexed CNOT gate with an extremely high fidelity of $\mathcal{F} = 93.8\%$.

We have further implemented a second generation source that has already demonstrated extremely low K-values. These allow for the interference between multiple PDC-events as well as the creation of highly pure single-mode squeezed states required for Gaussian boson sampling. The low propagation losses as well as the increased brightness of the source yield extreme squeezing strengths with more than 20 dB of generated squeezing. A comparison of the key performance indicators is displayed in Tab.I. From this we see, that we have successfully reached the goals of Task 1.1 and thus successfully deliver D1.1.

[1] C. S. Hamilton, R. Kruse, L. Sansoni, S. Barkhofen, C. Silberhorn, and I. Jex, Gaussian boson sampling, Phys. Rev. Lett. **119**, 170501 (2017).

[2] H.-S. Zhong, H. Wang, Y.-H. Deng, M.-C. Chen, L.-C. Peng, Y.-H. Luo, J. Qin, D. Wu, X. Ding, Y. Hu, P. Hu, X.-Y. Yang, W.-J. Zhang, H. Li, Y. Li, X. Jiang, L. Gan, G. Yang, L. You, Z. Wang, L. Li, N.-L. Liu, C.-Y. Lu, and J.-W. Pan, Quantum computational advantage using photons, Science **370**, 1460 (2020), https://www.science.org/doi/pdf/10.1126/science.abe8770.

[3] L. S. Madsen, F. Laudenbach, M. F. Askarani, F. Rortais, T. Vincent, J. F. F. Bulmer, F. M. Miatto, L. Neuhaus, L. G. Helt, M. J. Collins, A. E. Lita, T. Gerrits, S. W. Nam, V. D. Vaidya, M. Menotti, I. Dhand, Z. Vernon, N. Quesada, and J. Lavoie, enQuantum computational advantage with a programmable photonic processor, Nature **606**, 75 (2022).

[4] S. Yu, Z.-P. Zhong, Y. Fang, R. B. Patel, Q.-P. Li, W. Liu, Z. Li, L. Xu, S. Sagona-Stophel, E. Mer, S. E. Thomas, Y. Meng, Z.-P. Li, Y.-Z. Yang, Z.-A. Wang, N.-J. Guo, W.-H. Zhang, G. K. Tranmer, Y. Dong, Y.-T. Wang, J.-S. Tang, C.-F. Li, I. A. Walmsley, and G.-C. Guo, A universal programmable gaussian boson sampler for drug discovery, Nature Computational Science **3**, 839–848 (2023).

[5] A. Christ, K. Laiho, A. Eckstein, K. N. Cassemiro, and C. Silberhorn, Probing multimode squeezing with correlation functions, New Journal of Physics **13**, 033027 (2011).

[6] X. Shi, S. S. Mohanraj, V. Dhyani, A. A. Baiju, S. Wang, J. Sun, L. Zhou, A. Paterova, V. Leong, and D. Zhu, enEfficient photon-pair generation in layer-poled lithium niobate nanophotonic waveguides, Light Sci. Appl. **13**, 282 (2024).

[7] L. He, M. Zhang, A. Shams-Ansari, R. Zhu, C. Wang, and L. Marko, Low-loss fiber-to-chip interface for lithium niobate photonic integrated circuits, Opt. Lett. **44**, 2314 (2019).

[8] N. Yao, J. Zhou, R. Gao, J. Lin, M. Wang, Y. Cheng, W. Fang, and L. Tong, Efficient light coupling between an ultra-low loss lithium niobate waveguide and an adiabatically tapered single mode optical fiber, Opt. Express **28**, 12416 (2020).

[9] I. Krasnokutska, R. J. Chapman, J.-L. J. Tambasco, and A. Peruzzo, High coupling efficiency grating couplers on lithium niobate on insulator, Opt. Express **27**, 17681 (2019).

[10] A. B. U'Ren, C. Silberhorn, K. Banaszek, I. A. Walmsley, R. Erdmann, W. P. Grice, and M. G. Raymer, Generation of Pure-State Single-Photon Wavepackets by Conditional Preparation Based on Spontaneous Parametric Downconversion, Laser Physics **15**, 146 (2005).

[11] R. Regener and W. Sohler, Loss in low-finesse Ti:LiNbO3 optical waveguide resonators, Appl. Phys. B **36**, 143 (1985).

[12] P. B. Dixon, J. H. Shapiro, and F. N. C. Wong, Spectral engineering by gaussian phase-matching for quantum photonics, Opt. Express **21**, 5879 (2013).

[13] F. Graffitti, P. Barrow, M. Proietti, D. Kundys, and A. Fedrizzi, Independent high-purity photons created in domain-engineered crystals, Optica **5**, 514 (2018).

[14] M. Avenhaus, K. Laiho, M. V. Chekhova, and C. Silberhorn, Accessing higher order correlations in quantum optical states by time multiplexing, Phys. Rev. Lett. **104**, 063602 (2010).